Translational Oncology
www.transonc.com

Volume 6 Number 6 December 2013 pp. 685–696 685

Testing of SNS-032 in a Panel of Human Neuroblastoma Cell Lines with Acquired Resistance to a Broad Range of Drugs[1,2]

Nadine Löschmann*[,3], Martin Michaelis[†,3], Florian Rothweiler*, Richard Zehner[‡], Jaroslav Cinatl*, Yvonne Voges*, Mohsen Sharifi[§], Kristoffer Riecken[¶], Jochen Meyer[#], Andreas von Deimling[#], Iduna Fichtner, Taravat Ghafourian[§], Frank Westermann[††] and Jindrich Cinatl Jr***

*Institut für Medizinische Virologie, Klinikum der Goethe-Universität, Frankfurt am Main, Germany; [†]Centre for Molecular Processing and School of Biosciences, University of Kent, Canterbury, United Kingdom; [‡]Institut für Rechtsmedizin, Klinikum der Goethe-Universität, Frankfurt am Main, Germany; [§]Medway School of Pharmacy, Universities of Kent and Greenwich, Kent, United Kingdom; [¶]Forschungsabteilung Zell- und Gentherapie, Interdisziplinäre Klinik und Poliklinik für Stammzelltransplantation, Universitätsklinikum Hamburg-Eppendorf, Hamburg, Germany; [#]Department of Neuropathology, Ruprecht-Karls-University Heidelberg and Deutsches Krebsforschungszentrum, Heidelberg, Germany; **Max Delbrück Center for Molecular Medicine, Berlin, Germany; [††]Division of Tumor Genetics (B030), German Cancer Research Center, Heidelberg, Germany

Abstract

Novel treatment options are needed for the successful therapy of patients with high-risk neuroblastoma. Here, we investigated the cyclin-dependent kinase (CDK) inhibitor SNS-032 in a panel of 109 neuroblastoma cell lines consisting of 19 parental cell lines and 90 sublines with acquired resistance to 14 different anticancer drugs. Seventy-three percent of the investigated neuroblastoma cell lines and all four investigated primary tumor samples displayed concentrations that reduce cell viability by 50% in the range of the therapeutic plasma levels reported for SNS-032 (<754 nM). Sixty-two percent of the cell lines and two of the primary samples displayed concentrations that reduce cell viability by 90% in this concentration range. SNS-032 also impaired the growth of the multidrug-resistant cisplatin-adapted UKF-NB-3 subline UKF-NB-3^{r}CDDP^{1000} in mice. ABCB1 expression (but not ABCG2 expression) conferred resistance to SNS-032. The antineuroblastoma effects of SNS-032 did not depend on functional p53. The antineuroblastoma mechanism of SNS-032 included CDK7 and CDK9 inhibition–mediated suppression of RNA synthesis and subsequent depletion of antiapoptotic proteins with a fast turnover rate including X-linked inhibitor of apoptosis (XIAP), myeloid cell leukemia sequence 1 (Mcl-1), baculoviral IAP repeat containing 2 (BIRC2; cIAP-1), and survivin. In conclusion, CDK7 and CDK9 represent promising drug targets and SNS-032 represents a potential treatment option for neuroblastoma including therapy-refractory cases.

Translational Oncology (2013) 6, 685–696

Address all correspondence to: Jindrich Cinatl Jr, PhD, Paul Ehrlich-Str. 40, 60596 Frankfurt am Main, Germany. E-mail: Cinatl@em.uni-frankfurt.de

[1]The work was supported by the charity Hilfe für krebskranke Kinder Frankfurt e.V. and its trust Frankfurter Stiftung für krebskranke Kinder, by the Kent Cancer Trust, and by the Royal Society. Conflicts of interest: Nothing to declare.
[2]This article refers to supplementary materials, which are designated by Table W1 and Figures W1 to W5 and are available online at www.transonc.com.
[3]Equal contribution.
Received 8 August 2013; Revised 29 September 2013; Accepted 30 September 2013

Copyright © 2013 Neoplasia Press, Inc. All rights reserved 1944-7124/13/$25.00
DOI 10.1593/tlo.13544

Introduction

SNS-032 (BMS-387032) is an inhibitor of cyclin-dependent kinase 2 (CDK2), CDK7, and CDK9 that was shown to exert anticancer effects in leukemia, lymphoma, multiple myeloma, glioblastoma, lung cancer, osteosarcoma, and ovarian carcinoma cells [1–10], to exert chemopreventive effects in a mouse model of colorectal cancer [11], and to inhibit glioblastoma cell–induced angiogenesis [4]. The drug is under investigation in clinical trials for the treatment of different hematological and solid tumors [6,12–14]. Its mechanism of action was suggested to depend primarily on interference with CDK7 and CDK9 [5,12].

CDKs were suggested as therapeutic targets for the treatment of neuroblastoma [15,16], the most frequent solid extracranial pediatric cancer entity. About half of the patients are diagnosed with high-risk disease associated with overall survival rates below 50% despite myeloablative therapy and differentiation therapy using retinoids [17]. While many neuroblastomas respond initially well to therapy, acquired drug resistance represents a major problem [18,19].

Here, we investigated the effects of SNS-032 in a panel of 109 neuroblastoma cell lines consisting of 19 parental neuroblastoma cell lines and 90 sublines with acquired resistance to 14 different anticancer drugs. SNS-032 affected neuroblastoma cell viability in cell lines and primary tumor samples in therapeutic concentrations and in a xenograft mouse model. High ABCB1 expression impaired the efficacy of SNS-032, whereas it was modestly affected by ABCG2 expression and not influenced by the cellular p53 status. SNS-032 exerted its antineuroblastoma effects primarily through cytotoxic effects under involvement of CDK7 and particularly CDK9 as therapeutic targets.

Materials and Methods

Drugs

The compounds were purchased from the following sources: flubendazole from Enzo Life Sciences (Lörrach, Germany), SNS-032 and nutlin-3 from Selleck Chemicals through BIOZOL GmbH (Eching, Germany), vincristine and cisplatin from TEVA GmbH (Radebeul, Germany), doxorubicin from cell pharm (Bad Vilbel, Germany), melphalan and topotecan from GlaxoSmithKline GmbH and Co. KG (Munich, Germany), actinomycin D from Lundbeck Pharmaceuticals Ireland Limited (Dublin, Ireland), verapamil from Sigma-Aldrich (Munich, Germany), and Fumitremorgin C from Merck Millipore (Darmstadt, Germany).

Cells

The MYCN-amplified neuroblastoma cell lines UKF-NB-2, UKF-NB-3, UKF-NB-4, and UKF-NB-6 were established from patients with stage 4 neuroblastoma [20–23]. UKF-NB-3 clone 1 and UKF-NB-3 clone 3 are p53 wild-type single cell-derived sublines of UKF-NB-3 [24]. Be(2)C, IMR-32, SH-SY5Y, SK-N-AS, and SK-N-SH cells were obtained from American Type Culture Collection (ATCC; Manassas, VA); CHP-134, Kelly, LAN2, NGP, and NMB cells from DMSZ (Braunschweig, Germany); and GI-ME-N and LAN5 cells from ICLC (Genova, Italy). IMR-5, NLF, and SHEP cells were kindly provided by Dr Angelika Eggert (Universität Duisburg-Essen, Essen, Germany).

Neuroblastoma cell lines were adapted to growth in the presence of anticancer drugs by continuous exposure to increasing drug concentrations as described previously [21,22,24]. All neuroblastoma cell lines with acquired drug resistance were derived from the resistant cancer cell line (RCCL) collection. The corresponding concentrations that reduce cell viability by 50% (IC_{50}) for the parental cells and their drug-resistant sublines are provided in Table W1*A*.

All cells were propagated in Iscove's modified Dulbecco's medium (IMDM) supplemented with 10% fetal calf serum (FCS), 100 IU/ml penicillin, and 100 mg/ml streptomycin at 37°C. Cells were routinely tested for mycoplasma contamination and authenticated by short tandem repeat profiling.

p53-depleted neuroblastoma cells or neuroblastoma cells showing high expression of ABCB1 [also known as multidrug resistance protein 1 (MDR1) or P-glycoprotein] or ABCG2 [also known as breast cancer resistance protein (BCRP)] were established as described previously [25] using the Lentiviral Gene Ontology vector technology (www.lentigo-vectors.de).

Fresh neuroblastoma cells (MYCN amplified) were isolated from the bone marrow aspirate of four patients with metastasized International Neuroblastoma Staging System (INSS) stage 4 neuroblastoma following informed consent. Primary cells were cultivated in IMDM supplemented with 10% FCS, 100 IU/ml penicillin, and 100 mg/ml streptomycin at 37°C.

Mutation Analysis of p53

TP53 gene sequencing on cDNAs was performed as described previously [26] using the following four pairs of primers: TP53 Ex2-3-f GTGACACGCTTCCCTGGAT and TP53 Ex2-3-r TCATCTGGACCTGGGTCTTC; TP53 Ex4-5-f CCCTTCCCAGAAAACCTACC and TP53 Ex4-5-r CTCCGTCATGTGCTGTGACT; TP53 EX6-7f GTGCAGCTGTGGGTTGATT and TP53 Ex6-7r GGTGGTACAGTCAGAGCCAAC; Tp53 Ex8-9-f CCTCACCATCATCACACTGG and TP53 Ex8-9-rGTCTGGTCCTGAAGGGTGAA. In addition, all cell lines were examined for TP53 mutations by sequence analysis of genomic DNA. Each amplicon was sequenced bidirectionally.

Viability Assay

Cell viability was determined by the 3-(4,5-dimethylthiazol-2-yl)-2,5-diphenyltetrazolium bromide (MTT) dye reduction assay after 120-hour incubation and modified as described previously [24].

ABCB1 Expression and Rhodamine 123 Accumulation

ABCB1 expression and rhodamine accumulation were detected as described previously [25,27]. ABCB1 was detected by flow cytometry using a primary mouse anti-ABCB1 antibody (Alexis Biochemicals through AXXORA Deutschland, Lörrach, Germany) and a secondary phycoerythrin (PE)–labeled goat anti-mouse antibody (R&D Systems, Wiesbaden, Germany). Accumulation of the fluorescent ABCB1 substrate rhodamine 123 was determined using ABCB1-expressing UKF-NB-$3^{r}VCR^{10}$ cells. The cells were preincubated with SNS-032 or verapamil (ABCB1 inhibitor, positive control) for 30 minutes at 37°C before incubation with the fluorescent ABCB1 substrate rhodamine 123 (1 μM) for another 30 minutes. Then, the cells were washed twice with phosphate-buffered saline (PBS), fresh medium containing verapamil or SNS-032 was added, and the cellular fluorescence was analyzed after a further 30 minutes by flow cytometry.

ABCB1-Ligand Docking

ABCB1-ligand docking study was carried out using three-dimensional (3D) structures of mouse and human ABCB1 using MOE software (ver 2011.10; Chemical Computing Group Inc, Montreal, Quebec). The X-ray structures of the mouse homologue orthologue Abcb1a

[28] were obtained from the protein data bank (PDB codes: 3G60, 3G61, and 3G5U; http://www.rcsb.org). The proteins 3G60 and 3G61 are in complex with cyclic peptide inhibitors cyclic-tris-(*R*)-valineselenazole (QZ59-RRR) and cyclic-tris-(*S*)-valineselenazole (QZ59-SSS), whereas 3G5U is in the absence of a ligand. The homology model of the human ABCB1 structure was obtained from Bikadi et al. [29].

The protein and ligands were prepared for docking in MOE software. Protein structures were loaded into the software where the crystal parameters were retained, hydrogen atoms were added, and the proteins were titrated using default parameters of the software. To prepare the ligand, atomic charge and energy minimization was performed using self-consistent field (SCF) optimization (AM1 Hamiltonian). Maximum distance for nonbonded interacting atoms was 4.5 Å. In the MOE dock panel, the placement method was Triangle Matcher, the scoring methodology was set to London dG as the first and the second scoring functions, and the refinement methodology was set to MMFF94 force field. The mean energies and the backbone root mean square deviation of 30 best scoring poses were retained. The binding site was defined in MOE software using the co-crystallized hexapeptide inhibitors, QZ59-RRR and QZ59-SSS, as the guide or residues protected from methanethiosulfate (MTS) labeling by verapamil (suggesting verapamil binding site).

RNA Interference Experiments

Synthetic siRNA oligonucleotides targeting ABCB1, CDK7, or CDK9 (ON-TARGETplus SMARTpool siRNAs) were purchased from Dharmacon (Lafayette, CO). The nontargeting siRNA (ON-TARGETplus SMARTpool; Dharmacon) was used as a negative control. Transfections were performed using the Neon Transfection System (Invitrogen, Darmstadt, Germany) according to the manufacturer's protocol. UKF-NB-3 cells were grown to about 60% to 80% confluence and trypsinized, and 2×10^6 cells were resuspended in 200 µl of resuspension buffer containing 2.5 µM siRNA. Electroporation was performed in a pipette tip chamber with previously optimized adjustments (voltage of 1400; width of 20; two pulses). After electroporation, the cells were transferred into fibronectin (100 µg/ml)–coated six-well plates containing prewarmed IMDM plus 10% FCS.

Western Blot

Cells were lysed in Triton X-100 sample buffer and separated by sodium dodecyl sulfate–polyacrylamide gel electrophoresis. Proteins were detected using specific antibodies directed against β-actin (BioVision through BioCat GmbH, Heidelberg, Germany), CDK7, CDK9, X-linked inhibitor of apoptosis (XIAP), myeloid cell leukemia sequence 1 (Mcl-1), caspase 3, cleaved poly (ADP-ribose) polymerase (PARP; all from Cell Signaling Technology through New England Biolabs, Frankfurt am Main, Germany), RNA polymerase II, Ser-2–phosphorylated RNA polymerase II, Ser-5–phosphorylated RNA polymerase II (all from Abcam, Cambridge, United Kingdom), baculoviral IAP repeat containing 2 (cIAP-1), survivin (all from R&D Systems), and cIAP-2 (Epitomics through Abcam). Protein bands were visualized by enhanced chemiluminescence using a commercially available kit (Amersham, Freiburg, Germany).

RNA Synthesis Assay

Detection of global RNA synthesis was performed using the Click-iT RNA HCS Assay (Invitrogen) according to the manufacturer's protocol. Cells were seeded in 24-well cell culture plates and allowed to adhere overnight. Then, the cells were treated with the indicated drug concentrations for 6 hours. This was followed by 5-ethynyl uridine (1 mM) labeling for 1 hour at 37°C. The labeled cells were harvested in flow cytometer tubes, fixed with 4% formaldehyde, and permeabilized (0.1% Triton X-100) before incubation with the Click-iT reaction buffer (contains Alexa Flour azide) for 30 minutes at room temperature in the dark. The labeled RNA was quantified using a flow cytometer (FACSCanto; BD Biosciences, Heidelberg, Germany).

BAX Activity Assay

The cells were fixed and permeabilized using Cytofix/Cytoperm (BD Biosciences) according to the manufacturer's protocol. Then, the cells were incubated with an anti-BAX antibody (clone 6A7; BD Pharmingen, Heidelberg, Germany) for 30 minutes at 4°C that specifically recognizes a BAX binding site that is exclusively exposed on Bax activation in the mitochondrial membrane. After incubation with a secondary PE-labeled anti-mouse antibody for 30 minutes at 4°C, the percentage of cells displaying activated BAX was quantified by flow cytometry.

Mitochondrial Membrane Potential (Δψ) Analysis

The mitochondrial membrane potential ($\Delta\psi$) was examined using the BD MitoScreen/Flow Cytometry Mitochondrial Membrane Potential Detection Kit (BD Biosciences) according to the manufacturer's protocol. The cells were harvested and incubated with 5,5′,6,6′-tetrachloro-1,1′,3,3′-tetraethylbenzimidazolocarbocyanine I-/CI-salt (JC-1) for 15 minutes at 37°C. After washing twice with assay buffer, the $\Delta\psi$ was analyzed by flow cytometry.

Cytochrome c Release

The cytochrome *c* release in apoptotic cells was detected as described by Waterhouse and Trapani [30]. Cells were harvested, washed with cold PBS, pelleted, and permeabilized (10 ng/ml digitonin in PBS), so that cytochrome *c* released from the mitochondria in apoptotic cells could be washed away. On fixation with 4% formaldehyde, cells were incubated for 1 hour at room temperature with blocking buffer (0.05% saponin and 3% BSA in PBS), followed by incubation overnight at 4°C with primary anti–cytochrome *c* antibody (6H2.B4; BD Pharmingen). After incubation with secondary PE-labeled anti-mouse antibody for 40 minutes on ice, the cells were analyzed for their mitochondrial cytochrome *c* content by flow cytometry.

Caspase 3/7 Activity Assay

The activity of caspases 3 and 7 was examined using the Caspase-Glo 3/7 Assay (Promega GmbH, Mannheim, Germany) following the manufacturer's instructions. Cells were seeded in 96-well cell culture plates and allowed to adhere overnight. After drug treatment, the culture plates were adjusted to room temperature. Then, the cells were incubated for 5 minutes with the premixed substrate, and the luminescent signal was measured with a plate reader (Tecan, Crailsheim, Germany) for 30 cycles.

Detection of Sub-G_1 Cells

For the detection of sub-G_1 cells, the intracellular DNA was stained using propidium iodide (PI). Cells were harvested, washed with PBS, and fixed with 70% ethanol at −20°C overnight. After washing the cells with PBS twice, cells were stained for 30 minutes

with 500 µl of PI solution (20 µg/ml PI and 0.001% Triton X-100 in PBS) at room temperature in the dark. The DNA content of the cells was quantified by flow cytometry.

Xenograft Experiments

Mouse experiments were performed using male NMRI:nu/nu mice. UKF-NB-3^{r}CDDP^{1000} (1×10^{7}) cells were injected subcutaneously together with 50% Matrigel (BD Biosciences) into the right flank. When the tumors reached a palpable size, at day 21, mice were divided into two groups, each consisting of six animals. SNS-032 treatment was performed using 30 mg/kg SNS-032 dissolved in aqueous 2.1 mmol of tartaric acid solution intraperitoneally at days 21, 24, and 27. Control animals received aqueous 2.1 mmol of tartaric acid solution intraperitoneally at the same days. Tumor volumes were measured two times per week using a caliper. The tumor volumes were calculated

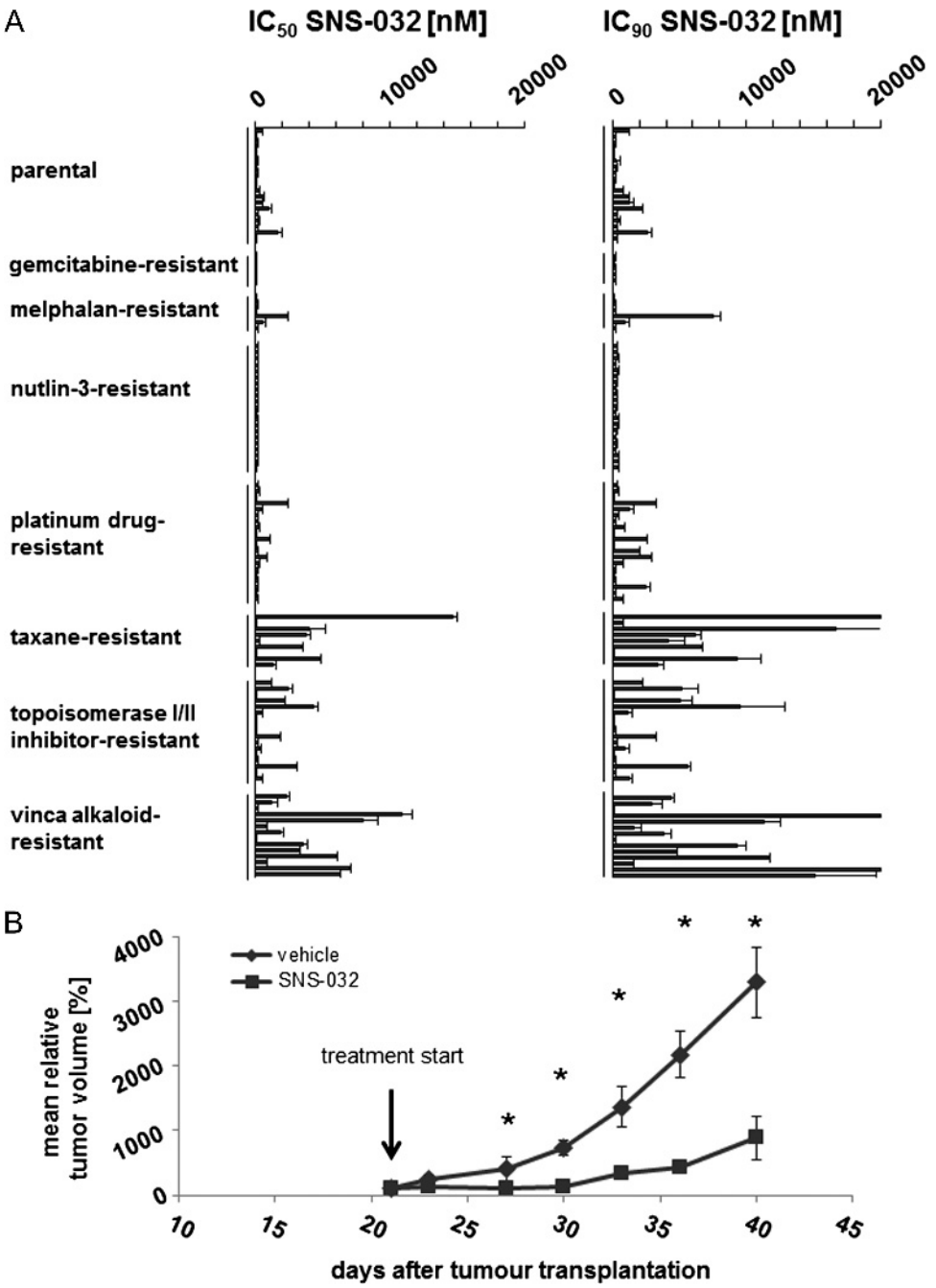

Figure 1. Antineuroblastoma effects of SNS-032 *in vitro* and *in vivo*. (A) Concentrations that reduce the viability of parental, chemosensitive neuroblastoma cell lines and their sublines with acquired resistance to a broad range of different anticancer drug classes by 50% (IC_{50}) or 90% (IC_{90}) as determined by MTT assay after a 5-day treatment period. (B) Effects of SNS-032 (30 mg/kg administered on days 21, 24, and 27) on the growth of subcutaneous UKF-NB-3^{r}CDDP^{1000} (UKF-NB-3 cells with acquired resistance to cisplatin) xenografts in comparison to vehicle controls. No tumors were palpable before day 21. *$P < .5$ compared to vehicle.

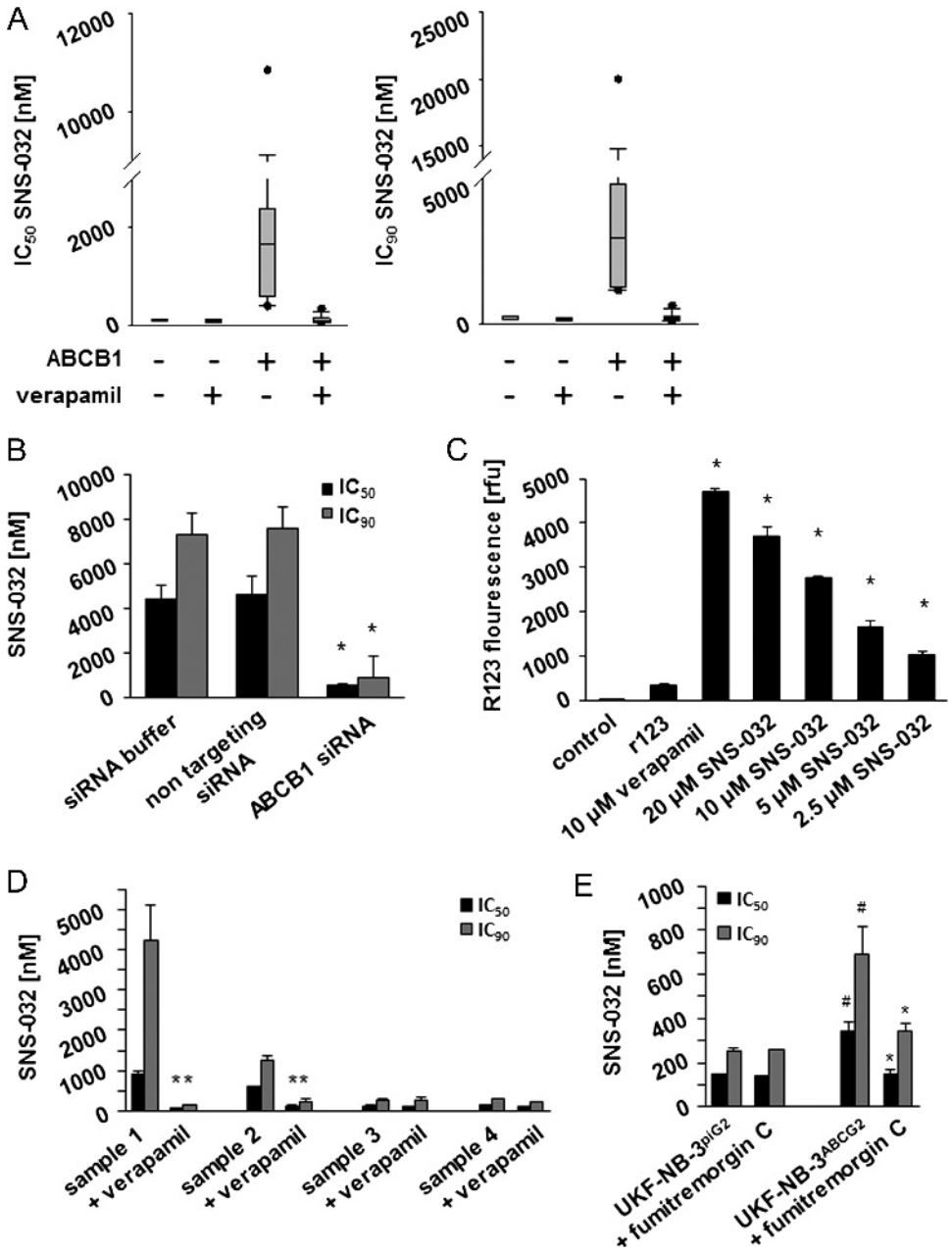

Figure 2. Effects of ABCB1 expression on neuroblastoma cell sensitivity to SNS-032. (A) Box plots indicating the SNS-032 concentrations that reduce the viability of low and high ABCB1-expressing cells in the absence or presence of the ABCB1 inhibitor verapamil (10 μM) by 50% (IC_{50}) or 90% (IC_{90}) as indicated by MTT assay after 5 days of incubation. (B) Effects of siRNA-mediated depletion of ABCB1 on the SNS-032 concentrations that reduce UKF-NB-3^{ABCB1} cell viability by 50% (IC_{50}) or 90% (IC_{90}) as indicated by MTT assay 48 hours after transfection. *$P < .05$ relative to siRNA buffer and nontargeting siRNA. (C) Effects of verapamil or SNS-032 on the accumulation of the fluorescent ABCB1 substrate rhodamine 123 in ABCB1-expressing UKF-NB-$3^{r}VCR^{10}$ cells; *$P < .05$ relative to rhodamine 123 alone. (D) Effects of SNS-032 on the viability of primary neuroblastoma cells in the absence or presence of verapamil (10 μM), *$P < .05$ relative to SNS-032 alone. (E) Effect of SNS-032 on the expression of UKF-NB-3 cells transduced with a lentiviral vector encoding for ABCG2 (UKF-NB-3^{ABCG2}) or a control vector (UKF-NB-3^{piG2}) in the absence or presence of the ABCG2 inhibitor Fumitremorgin C (10 μM). *$P < .05$ relative to non–Fumitremorgin C–treated cells; $^{\#}P < .05$ relative to UKF-NB-3^{piG2} cells.

by the formula volume = length × $width^2/2$. The experiments were terminated when the control tumors reached a size > 1 cm^2.

The animal experiments were performed according to the German Animal Protection Law and with approval from the responsible authorities (LaGeSo, Berlin, Germany). The procedures were consistent and in compliance with the United Kingdom Coordinating Committee on Cancer Research (UKCCCR) guidelines.

Results

Anticancer Effects of SNS-032 on Neuroblastoma Cells In Vitro *and* In Vivo

SNS-032 was tested in a panel of 109 neuroblastoma cell lines consisting of 19 parental neuroblastoma cell lines and 90 drug-adapted sublines (Figure 1*A* and Table W1*B*). The IC_{50} values ranged from

58.3 (NLF^{r}PCL^{20}) to 14,615 nM (IMR-5^{r}DOCE^{20}), and the concentrations that reduce cell viability by 90% (IC_{90}) ranged from 106.4 (NLF^{r}PCL^{20}) to >20,000 nM (IMR-5^{r}DOCE^{20}, SHEP^{r}VCR^{1}). In the parental cells, the IC_{50} values ranged from 95.7 (NGP) to 1671 nM (UKF-NB-4), and the IC_{90} values ranged from 152.4 nM (NLF) to 2611 nM (UKF-NB-4).

In the drug-adapted cell lines, there was, in general, a good correlation between the relative fold changes in the SNS-032 IC_{50} (IC_{50} drug-adapted cell/IC_{50} parental cell) and IC_{90} values (IC_{90} drug-adapted cell/IC_{90} parental cell) between parental and corresponding drug-adapted cell lines. A substantial difference was detected only in NLF^{r}DOCE^{20} (IC_{50} NLF^{r}DOCE^{20}/IC_{50} NLF = 1.37; IC_{90} NLF^{r}DOCE^{20}/IC_{90} NLF = 4.66), UKF-NB-2^{r}CARBO^{2000} (IC_{50} UKF-NB-2^{r}CARBO^{2000}/IC_{50} UKF-NB-2 = 0.68; IC_{90} UKF-NB-2^{r}CARBO^{2000}/IC_{90} UKF-NB-2 = 3.99), and UKF-NB-2^{r}OXALI^{600} (IC_{50} UKF-NB-2^{r}OXALI^{600}/IC_{50} UKF-NB-2 = 0.78; IC_{90} UKF-NB-2^{r}OXALI^{600}/IC_{90} UKF-NB-2 = 4.77) cells compared to the parental cells.

A significant fraction of the drug-adapted neuroblastoma cell lines showed a similar SNS-032 sensitivity like the corresponding parental cells. Fifty-five of the 90 drug-adapted cell lines (61%) displayed IC_{50} drug-adapted cell line/IC_{50} parental cell line and IC_{90} drug-adapted cell line/IC_{90} parental cell line ratios between 0.5 and 2.0. Acquired resistance to tubulin-binding agents and doxorubicin appeared to result generally in cross-resistance to SNS-032. Seven of 8 taxane (docetaxel, paclitaxel)–adapted cell lines, 12 of 14 vinca alkaloid (vincristine, vinblastine, vinorelbine)–adapted cell lines, and 4 of 5 doxorubicin-resistant cell lines displayed ratios of the IC_{90} resistant cell/IC_{90} parental cell > 2 (Figure 1*A* and Table W1*B*). All five gemcitabine-resistant sublines remained SNS-032 sensitive (ratios of the IC_{90} resistant cell/IC_{90} parental cell $\leq$ 2), whereas a fraction of the cell lines displaying acquired resistance to platinum drugs (9 of 20), etoposide (2 of 6), melphalan (2 of 6), or topotecan (2 of 5) displayed also decreased sensitivity to SNS-032.

The anticancer effects of SNS-032 were further investigated in primary neuroblastoma cells isolated from the bone marrow of four patients with metastasized INSS stage 4 (Table W1*C*). The effective concentrations were in the range of those detected in the neuroblastoma cell lines.

The effect of SNS-032 on tumor growth in the xenograft model was investigated using the multidrug-resistant cisplatin-adapted UKF-NB-3 subline UKF-NB-3^{r}CDDP^{1000}. UKF-NB-3^{r}CDDP^{1000} cells showed a remarkable cross-resistance (IC_{90} UKF-NB-3^{r}CDDP^{1000}/IC_{90} UKF-NB-3) to doxorubicin (5.2-fold), melphalan (13.9-fold), and topotecan (2.4-fold), a moderate cross-resistance to vincristine (1.9-fold), but no cross-resistance to SNS-032 (0.7-fold; Table W1*D*).

SNS-032 (30 mg/kg administered on days 1, 4, and 7) significantly inhibited UKF-NB-3^{r}CDDP^{1000} xenograft growth without substantially influencing mice body weights. Mean relative tumor volumes are shown in Figure 1*B*. Individual tumor growth curves and mouse body weights are presented in Figure W1.

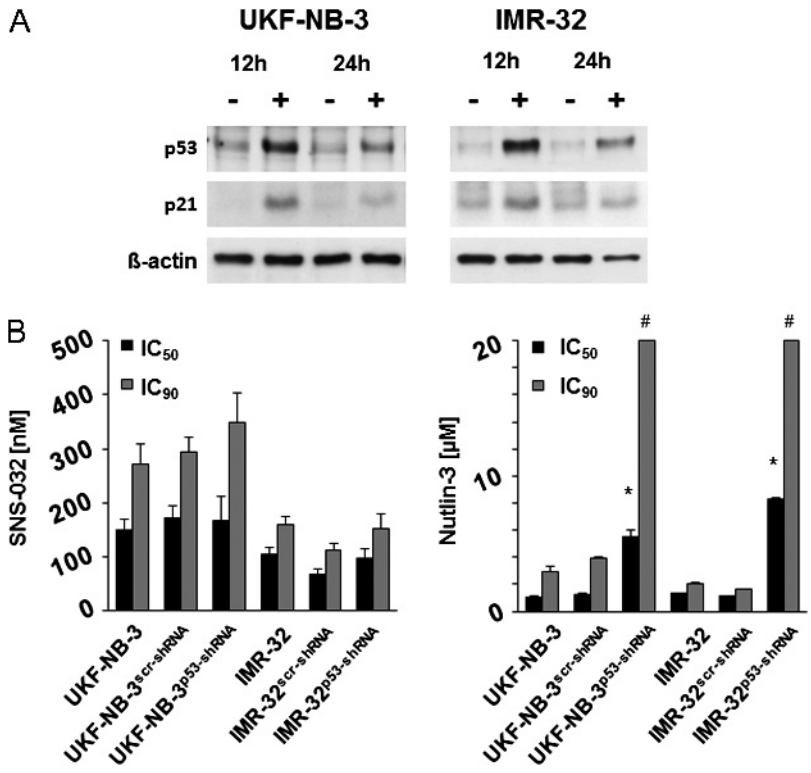

Figure 3. Relevance of functional p53 for the SNS-032–mediated antineuroblastoma effects. (A) SNS-032 (0.3 μM)–induced induction of p53 and p21 expression in neuroblastoma cells. (B) Concentrations that reduce neuroblastoma cell viability by 50% (IC_{50}) or 90% (IC_{90}) in neuroblastoma cells in the absence or presence of functional p53; p53 was depleted in UKF-NB-3$^{p53\text{-}shRNA}$ and IMR-32$^{p53\text{-}shRNA}$ cells using a lentiviral vector. UKF-NB-3$^{scr\text{-}shRNA}$ and IMR-32$^{scr\text{-}shRNA}$ were transduced with a control vector encoding for nontargeted scrambled shRNA. The p53 activator nutlin-3 that is known to depend on functional p53 in our model system was used as control. *$P < .05$ relative to the nontargeting shRNA control; $^{\#}IC_{90} > 20$ μM.

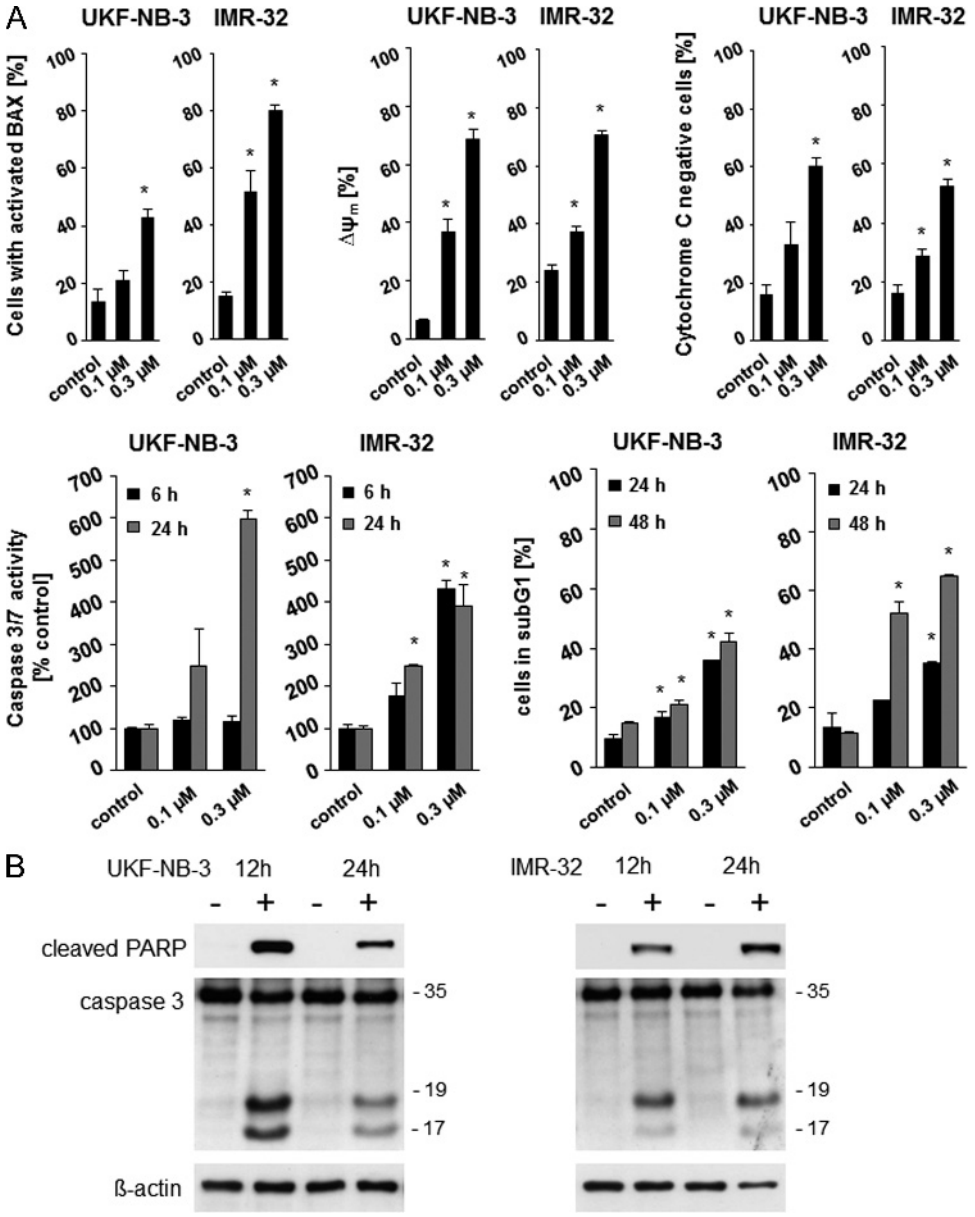

Figure 4. Apoptosis induction by SNS-032 in neuroblastoma cells. (A) BAX activation, mitochondrial membrane potential ($\Delta\psi$), fraction of cytochrome-negative cells, enzymatic caspase 3/7 activity, and fraction of sub-G_1 cells in SNS-032–treated UKF-NB-3 and IMR-32 cells. *$P < .05$ relative to nontreated control. (B) Western blots indicating SNS-032 (300 nM)–induced PARP and caspase-3 cleavage in UKF-NB-3 and IMR-32 cells.

Influence of ABCB1 and ABCG2 Expression on Cellular SNS-032 Sensitivity

Many kinase inhibitors were shown to interfere with ABC transporters including ABCB1 and ABCG2 [31,32]. SNS-032 had previously been suggested to be a substrate of ABCB1 [33]. In accordance, our docking studies suggested a strong interaction of SNS-032 with ABCB1. SNS-032 was docked into the homology model of human ABCB1 and the three X-ray structures of mouse Abcb1a, with the binding sites defined using the positions of the co-crystallized ligands, QZ59-RRR and QZ59-SSS (amino acid residues within 4.5-Å distance), and the verapamil binding site (residues protected from MTS labeling by verapamil) as described by Aller et al. [28]. The detailed procedures and results of our docking study are presented in Figure W2.

Indeed, we detected higher SNS-032 IC_{50} values in neuroblastoma cells that display high ABCB1 expression than in neuroblastoma cells characterized by low ABCB1 expression (Figure 2*A* and Table W1*E*). The ABCB1 inhibitor verapamil sensitized cells that express high ABCB1 levels to SNS-032 but affected SNS-032 sensitivity in cells that express low ABCB1 levels to a much lower extent (Figure 2*A* and Table W1*E*). Transduction of low ABCB1-expressing UKF-NB-3 cells with a lentiviral vector encoding for ABCB1 (UKF-NB-3^{ABCB1}) resulted in a 48-fold increase in the SNS-032 IC_{90} (Table W1*F*) and RNAi-mediated depletion of ABCB1 in UKF-NB-3^{ABCB1} cells or addition of the ABCB1 inhibitor verapamil resulted in their resensitization to SNS-032 (Figures 2*B* and W3 and Table W1*F*). Moreover, SNS-032 increased the accumulation of the fluorescent ABCB1 substrate

rhodamine 123 in highly ABCB1-expressing UKF-NB-3^{r}VCR^{10} cells in a concentration-dependent manner (Figure 2*C*). Notably, two of the four primary samples (samples 1 and 2) expressed ABCB1 (Figure W4) and were sensitized by the ABCB1 inhibitor verapamil (10 μM) to SNS-032 (Figure 2*D* and Table W1*C*).

Taken together, these data confirm that the activity of SNS-032 is affected by ABCB1 expression and that SNS-032 affects ABCB1 function.

ABCG2 also interfered with the SNS-032 efficacy, and the ABCG2 inhibitor Fumitremorgin C sensitized ABCG2-expressing cells to SNS-032, however, to a much lesser extent (Figure 2*E* and Table W1*G*).

Influence of p53 on the Neuroblastoma Cell Response to SNS-032

SNS-032 treatment induced p53 accumulation and accumulation of the p53 target gene *p21* in UKF-NB-3 and IMR-32 cells (Figure 3*A*). To investigate the role of p53 within the cellular response to SNS-032, we depleted p53 in the p53 wild-type neuroblastoma cell lines UKF-NB-3 and IMR-32 using a lentiviral vector encoding for p53 shRNA as described before [25]. The p53-depleted cells displayed decreased sensitivity to the murine double minute 2 (MDM2) inhibitor nutlin-3 that exerts its antineuroblastoma effects through induction of p53-mediated apoptosis [24,27,34] but not to SNS-032 (Figure 3*B*). Moreover, p53 depletion reduced the UKF-NB-3 cell sensitivity to the cytotoxic anticancer drugs actinomycin D, cisplatin, melphalan, and vincristine (Table W1*H*). Notably, SNS-032 exerted also similar effects in parental UKF-NB-3 and UKF-NB-6 cells and its sublines adapted to nutlin-3 harboring different p53 mutations (Figure 1*A* and Table W1, *B* and *J*). Therefore, p53 does not appear to be critical for the antineuroblastoma effects exerted by SNS-032.

Influence of SNS-032 on Neuroblastoma Cell Proliferation and Death

SNS-032 treatment caused clear features of apoptotic cell death in neuroblastoma cells. SNS-032 induced BAX activation, reduced the mitochondrial membrane potential, provoked mitochondrial cytochrome *c* release, enhanced the enzymatic caspase 3/7 activity, and increased the number of sub-G_1 cells in a concentration-dependent manner in UKF-NB-3 and IMR-32 cells (Figure 4*A*). Western blots

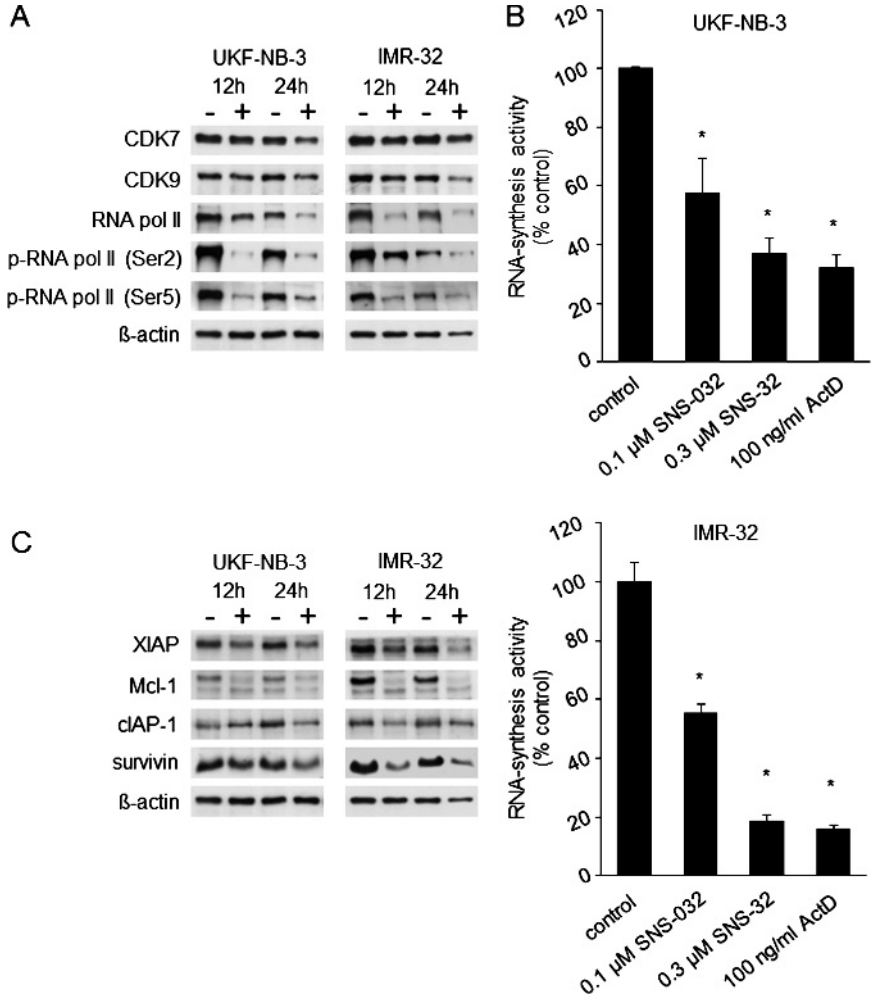

Figure 5. Effects of SNS-032 on CDK7 and CDK9 signaling, RNA synthesis, and expression of antiapoptotic proteins in neuroblastoma cells. (A) Effects of SNS-032 (300 nM) on CDK7 expression and the expression and phosphorylation [p-RNA pol II (Ser-5)] of its downstream RNA polymerase II (RNA pol II) and on CDK9 expression and the expression and phosphorylation [p-RNA pol II (Ser-2)] of its downstream RNA pol II. (B) UKF-NB-3 or IMR-32 cells were treated for 6 hours with SNS-032 or actinomycin D (ActD, positive control for RNA synthesis inhibition) before the determination of RNA synthesis activity. *$P < .05$ relative to nontreated control. (C) Western blots indicating cellular levels of antiapoptotic proteins with high turnover rates in SNS-032 (300 nM)–treated neuroblastoma cells.

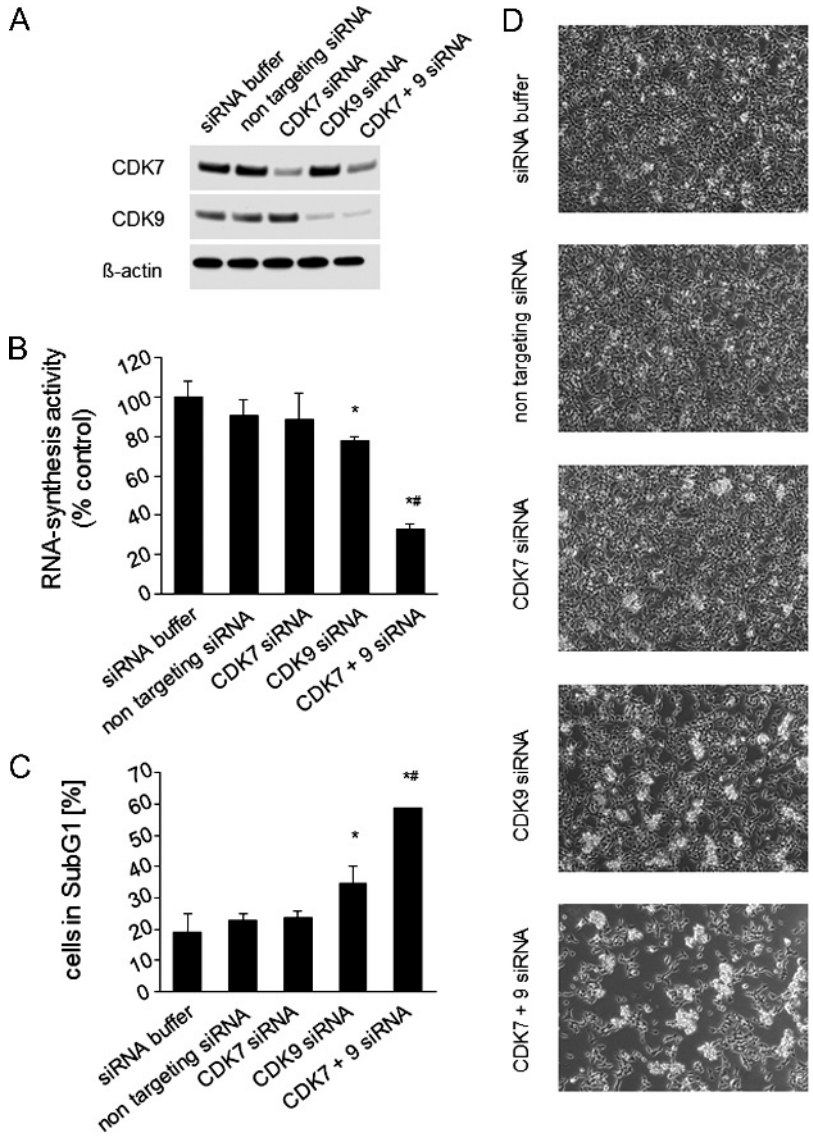

Figure 6. Effects of RNAi-mediated depletion of CDK7 and/or CDK9 on UKF-NB-3 neuroblastoma cell viability. (A) Western blot showing siRNA-mediated depletion of CDK7 and/or CDK9 in UKF-NB-3 cells as determined 48 hours after. (B) Effects of CDK7 and/or CDK9 depletion on RNA synthesis 48 hours after transfection; $^{*}P < .05$ relative to nontargeting siRNA, $^{\#}P < .05$ relative to CDK9 siRNA. (C) Effects of CDK7 and/or CDK9 depletion on the number of sub-G_1 cells 48 hours after transfection; $^{*}P < .05$ relative to nontargeting siRNA, $^{\#}P < .05$ relative to CDK9 siRNA. (D) Representative photographs showing cancer cell cultures 48 hours after transfection.

detected caspase 3 cleavage indicating caspase 3 activation and PARP cleavage, an additional characteristic of apoptosis (Figure 4*B*).

Effects of SNS-032 on CDK7 and CDK9

SNS-032 reduced CDK7 and CDK9 expression in the neuroblastoma cell lines UKF-NB-3 and IMR-32 and interfered with the downstream signaling of these CDKs (Figure 5). CDK7 and CDK9 are involved in transcription. CDK7 phosphorylates RNA polymerase II at Ser-5 as a member of the transcription factor complex TFIIH and promotes transcription initiation [35]. CDK9 phosphorylates RNA polymerase II at Ser-2 as a member of the elongation factor complex P-TEFb and promotes elongation [36]. SNS-032 interfered with RNA polymerase II phosphorylation at both phosphorylation sides (Figure 5*A*). In accordance with its effects on RNA polymerase II, SNS-032 also inhibited RNA synthesis in a concentration-dependent manner in UKF-NB-3 and IMR-32 cells (Figure 5*B*).

In chronic myeloid leukemia cells, RNA synthesis inhibition by SNS-032 resulted in decreased cellular levels of the antiapoptotic proteins Mcl-1 and XIAP that have a high turnover rate [5]. Similarly, SNS-032 reduced the levels of Mcl-1, XIAP, cIAP, and survivin in neuroblastoma cells (Figure 5*C*).

Next, we investigated the effects of siRNA-mediated depletion of CDK7 and CDK9 on RNA synthesis and viability in UKF-NB-3 cells. Results revealed that inhibition of CDK9 resulted in the strongest effects, which were further enhanced in combination with CDK7 (Figure 6).

Discussion

Acquired drug resistance represents a major problem in the successful treatment of neuroblastoma [18,19]. Therefore, additional treatment

options are needed to improve the therapy outcome for patients that cannot be treated satisfactorily by the current therapy regimens. Here, we investigated the effects of SNS-032 in a panel of 109 neuroblastoma cell lines consisting of 19 parental neuroblastoma cell lines and 90 sublines with acquired resistance to 14 different anticancer drugs. The results indicated that neuroblastoma cell resistance acquisition to certain drugs is more likely to result in cross-resistance to SNS-032 than resistance acquisition to other drugs. The resistance acquisition to taxanes, vinca alkaloids, and doxorubicin appeared to be in general (but not always) associated with a reduced sensitivity to SNS-032. All five gemcitabine-resistant cell lines retained sensitivity to SNS-032, whereas half or less of the platinum drug-, melphalan-, etoposide-, or topotecan-resistant cell lines displayed cross-resistance to SNS-032. These findings confirm previous assumptions that a drug needs to be investigated in many cancer cell lines to receive a reasonable idea of its possible therapeutic potential in a certain cancer entity [37]. Moreover, our results are in accordance with previous studies performed in mantle cell lymphoma cells that had indicated the SNS-032 response to depend on the biologic context of each individual cell line [7].

Therapeutic SNS-032 plasma concentrations were reported to range from 176 to 754 nM in clinical trials in adults [12]. Because data on the SNS-032 pharmacokinetics in children are missing, we used the data derived from adults to analyze our findings. The viability of a significant fraction of the investigated cell lines was affected in this concentration range. Fifty-two of the investigated 109 cell lines (48%) displayed an SNS-032 IC_{50} value lower than 176 nM, and 14 cell lines (13%) displayed an SNS-032 IC_{90} value lower than 176 nM. Eighty of the 109 cell lines (73%) displayed an IC_{50} smaller than 754 nM, and 68 (62%) displayed an IC_{90} below 754 nM. Among the parental cell lines, 9 of 19 cell lines (47%) displayed an IC_{50} below 176 nM and 3 (16%) displayed an IC_{90} below 176 nM. Seventeen parental cell lines (89%) displayed an IC_{50} below 754 nM, and 13 (68%) displayed an IC_{90} below 754 nM. Moreover, all four primary neuroblastoma samples had IC_{50} values below 754 nM, and the IC_{90} values of two of the samples were also below 754 nM. On the basis of these findings, SNS-032 may represent a treatment option for a fraction of patients with neuroblastoma. In animal experiments, SNS-032 inhibited the growth of cisplatin-resistant UKF-NB-3^{r}CDDP^{1000} cells that display cross-resistance to a range of anticancer drugs. This confirms that SNS-032 is also active against neuroblastoma under *in vivo* conditions. Possibly, the *in vivo* efficacy of SNS-032 could be further enhanced by optimized application schemes in our model. However, it is unlikely that a compound would be introduced clinically as a monotherapy for recurrent neuroblastoma. Our preliminary results suggest that SNS-032 may exert enhanced antineuroblastoma effects in combination with cytotoxic anticancer drugs including cisplatin, melphalan, and topotecan (Figure W5). Therefore, the focus of follow-up studies should probably be on effective combination therapies.

Pharmacokinetic studies in rats had indicated that SNS-032 was an ABCB1 substrate [33]. We performed *in silico* docking studies that confirmed SNS-032 to be a potential ABCB1 substrate. Indeed, ABCB1 expression was correlated with decreased neuroblastoma cell sensitivity to SNS-032. Pharmacological inhibition or RNAi-mediated depletion of ABCB1 strongly sensitized ABCB1-expressing cells to SNS-032. ABCB1 may be a dominant SNS-032 resistance mechanism in neuroblastoma. In the presence of the ABCB1 inhibitor verapamil, the IC_{50} values of all 30 neuroblastoma cell lines that had displayed IC_{50} values > 754 nM were reduced to values < 754 nM. Moreover, the IC_{90} values of 39 of the 41 cell lines (95%) that had IC_{90} values > 754 nM were reduced to therapeutic concentrations < 754 nM in the presence of verapamil (Table W1*K*). In contrast, ABCG2 expression only modestly affected neuroblastoma cell sensitivity to SNS-032. This demonstrates that ABCB1 expression is a major SNS-032 resistance mechanism in neuroblastoma. The clinical role of ABCB1 expression in neuroblastoma remains unclear [18,38]. At diagnosis, few neuroblastoma cells appear to express ABCB1 and the prognostic relevance of ABCB1 expression appears to be limited [39,40]. However, ABCB1 expression might represent an acquired resistance mechanism in neuroblastoma [41].

The formation of p53 mutations was suggested to be an acquired resistance mechanism in neuroblastoma [19]. In general, p53 mutations were described to be rare in neuroblastoma. However, while p53 was found mutated in only 2% of neuroblastomas at diagnosis, p53 mutations were detected in about 15% of neuroblastomas at relapse [19,42,43]. Moreover, p53 mutations represented an independent prognostic factor for overall survival in neuroblastoma [19,42]. In accordance, the analysis of two cell lines derived from the same patient revealed that the cell line established from the primary tumor before cytotoxic therapy harbored wild-type p53, whereas the cell line derived after cytotoxic therapy harbored a p53 mutation [44]. These findings are also consistent with studies in preclinical neuroblastoma models demonstrating that the loss of p53 function is associated with resistance to multiple anticancer drugs and radiotherapy and that resistance acquisition to anticancer drugs may be associated with p53 mutations [19,22,24,45–48]. In addition, abnormalities in the p53/MDM2/p14^{ARF} pathway different from p53 mutations were detected in 35% of the neuroblastoma samples indicating that p53 signaling is substantially impaired by varying mechanisms in 50% of neuroblastomas [19,42]. Consequently, drugs that exert their antineuroblastoma effects independently of the presence of functional p53 are highly desirable. Notably, SNS-032 (but not the cytotoxic drugs actinomycin D, cisplatin, melphalan, or vincristine) displayed the same efficacy in neuroblastoma cells in the absence or presence of functional p53.

The anticancer mechanism of SNS-032 in neuroblastoma cells apparently resembles the anticancer mechanism that was described for SNS-032 in chronic myeloid leukemia cells [5]. SNS-032 inhibited CDK7 and CDK9 expression and reduced the phosphorylation of the CDK7 and CDK9 downstream RNA polymerase II. This resulted in the suppression of RNA synthesis and decreased cellular levels of antiapoptotic proteins with a high turnover rate including Mcl-1, XIAP, cIAP-1, and survivin. RNAi-mediated depletion of CDK9 (but not of CDK7) resulted in substantial antineuroblastoma effects. Therefore, our findings appear to be in line with recent studies suggesting CDK9 to be a critical anticancer drug target among the CDKs [49]. Notably, the effects of CDK9 depletion were significantly further enhanced by simultaneous CDK7 depletion.

Taken together, SNS-032 and other therapy strategies that target CDK7 and CDK9 represent potential treatment options for neuroblastoma including therapy-refractory cases.

Acknowledgments

The authors thank Gesa Meincke, Eva Wagner, and Sebastian Grothe for technical support.

References

[1] Misra RN, Xiao HY, Kim KS, Lu S, Han WC, Barbosa SA, Hunt JT, Rawlins DB, Shan W, Ahmed SZ, et al. (2004). *N*-(cycloalkylamino)acyl-2-aminothiazole

inhibitors of cyclin-dependent kinase 2. *N*-[5-[[[5-(1,1-dimethylethyl)-2-oxazolyl] methyl]thio]-2-thiazolyl]-4-piperidinecarboxamide (BMS-387032), a highly efficacious and selective antitumor agent. *J Med Chem* **47**, 1719–1728.

[2] Mukhopadhyay P, Ali MA, Nandi A, Carreon P, Choy H, and Saha D (2006). The cyclin-dependent kinase 2 inhibitor down-regulates interleukin-1β-mediated induction of cyclooxygenase-2 expression in human lung carcinoma cells. *Cancer Res* **66**, 1758–1766.

[3] Scrace SF, Kierstan P, Borgognoni J, Wang LZ, Denny S, Wayne J, Bentley C, Cansfield AD, Jackson PS, Lockie AM, et al. (2008). Transient treatment with CDK inhibitors eliminates proliferative potential even when their abilities to evoke apoptosis and DNA damage are blocked. *Cell Cycle* **7**, 3898–3907.

[4] Ali MA, Choy H, Habib AA, and Saha D (2007). SNS-032 prevents tumor cell–induced angiogenesis by inhibiting vascular endothelial growth factor. *Neoplasia* **9**, 370–381.

[5] Chen R, Wierda WG, Chubb S, Hawtin RE, Fox JA, Keating MJ, Gandhi V, and Plunkett W (2009). Mechanism of action of SNS-032, a novel cyclin-dependent kinase inhibitor, in chronic lymphocytic leukemia. *Blood* **113**, 4637–4645.

[6] Conroy A, Stockett DE, Walker D, Arkin MR, Hoch U, Fox JA, and Hawtin RE (2009). SNS-032 is a potent and selective CDK 2, 7 and 9 inhibitor that drives target modulation in patient samples. *Cancer Chemother Pharmacol* **64**, 723–732.

[7] Chen R, Chubb S, Cheng T, Hawtin RE, Gandhi V, and Plunkett W (2010). Responses in mantle cell lymphoma cells to SNS-032 depend on the biological context of each cell line. *Cancer Res* **70**, 6587–6597.

[8] Kruse U, Pallasch CP, Bantscheff M, Eberhard D, Frenzel L, Ghidelli S, Maier SK, Werner T, Wendtner CM, and Drewes G (2011). Chemoproteomics-based kinome profiling and target deconvolution of clinical multi-kinase inhibitors in primary chronic lymphocytic leukemia cells. *Leukemia* **25**, 89–100.

[9] Walsby E, Lazenby M, Pepper C, and Burnett AK (2011). The cyclin-dependent kinase inhibitor SNS-032 has single agent activity in AML cells and is highly synergistic with cytarabine. *Leukemia* **25**, 411–419.

[10] Wu Y, Chen C, Sun X, Shi X, Jin B, Ding K, Yeung SC, and Pan J (2012). Cyclin-dependent kinase 7/9 inhibitor SNS-032 abrogates FIP1-like-1 platelet-derived growth factor receptor α and bcr-abl oncogene addiction in malignant hematologic cells. *Clin Cancer Res* **18**, 1966–1978.

[11] Boquoi A, Chen T, and Enders GH (2009). Chemoprevention of mouse intestinal tumorigenesis by the cyclin-dependent kinase inhibitor SNS-032. *Cancer Prev Res (Phila)* **2**, 800–806.

[12] Heath EI, Bible K, Martell RE, Adelman DC, and Lorusso PM (2008). A phase 1 study of SNS-032 (formerly BMS-387032), a potent inhibitor of cyclin-dependent kinases 2, 7 and 9 administered as a single oral dose and weekly infusion in patients with metastatic refractory solid tumors. *Invest New Drugs* **26**, 59–65.

[13] Tong WG, Chen R, Plunkett W, Siegel D, Sinha R, Harvey RD, Badros AZ, Popplewell L, Coutre S, Fox JA, et al. (2010). Phase I and pharmacologic study of SNS-032, a potent and selective Cdk2, 7, and 9 inhibitor, in patients with advanced chronic lymphocytic leukemia and multiple myeloma. *J Clin Oncol* **28**, 3015–3022.

[14] Robak P and Robak T (2012). A targeted therapy for protein and lipid kinases in chronic lymphocytic leukemia. *Curr Med Chem* **19**, 5294–5318.

[15] Bettayeb K, Baunbæk D, Delehouze C, Loaëc N, Hole AJ, Baumli S, Endicott JA, Douc-Rasy S, Bénard J, Oumata N, et al. (2010). CDK inhibitors roscovitine and CR8 trigger Mcl-1 down-regulation and apoptotic cell death in neuroblastoma cells. *Genes Cancer* **1**, 369–380.

[16] Garrofé-Ochoa X, Cosialls AM, Ribas J, Gil J, and Boix J (2011). Transcriptional modulation of apoptosis regulators by roscovitine and related compounds. *Apoptosis* **16**, 660–670.

[17] Maris JM (2010). Recent advances in neuroblastoma. *N Engl J Med* **362**, 2202–2211.

[18] Brodeur GM (2011). Knowing your ABCCs: novel functions of ABCC transporters. *J Natl Cancer Inst* **103**, 1207–1208.

[19] Chen L and Tweddle DA (2012). *p53*, *SKP2*, and *DKK3* as MYCN target genes and their potential therapeutic significance. *Front Oncol* **2**, 173.

[20] Cinatl J Jr, Vogel JU, Cinatl J, Weber B, Rabenau H, Novak M, Kornhuber B, and Doerr HW (1996). Long-term productive human cytomegalovirus infection of a human neuroblastoma cell line. *Int J Cancer* **65**, 90–96.

[21] Kotchetkov R, Cinatl J, Blaheta R, Vogel JU, Karaskova J, Squire J, Hernáiz Driever P, Klingebiel T, and Cinatl J Jr (2003). Development of resistance to vincristine and doxorubicin in neuroblastoma alters malignant properties and induces additional karyotype changes: a preclinical model. *Int J Cancer* **104**, 36–43.

[22] Kotchetkov R, Driever PH, Cinatl J, Michaelis M, Karaskova J, Blaheta R, Squire JA, Von Deimling A, Moog J, and Cinatl J Jr (2005). Increased malignant behavior in neuroblastoma cells with acquired multi-drug resistance does not depend on P-gp expression. *Int J Oncol* **27**, 1029–1037.

[23] Michaelis M, Kleinschmidt MC, Barth S, Rothweiler F, Geiler J, Breitling R, Mayer B, Deubzer H, Witt O, Kreuter J, et al. (2010). Anti-cancer effects of artesunate in a panel of chemoresistant neuroblastoma cell lines. *Biochem Pharmacol* **79**, 130–136.

[24] Michaelis M, Rothweiler F, Barth S, Cinatl J, van Rikxoort M, Löschmann N, Voges Y, Breitling R, von Deimling A, Rödel F, et al. (2011). Adaptation of cancer cells from different entities to the MDM2 inhibitor nutlin-3 results in the emergence of p53-mutated multi-drug-resistant cancer cells. *Cell Death Dis* **2**, e243.

[25] Rothweiler F, Michaelis M, Brauer P, Otte J, Weber K, Fehse B, Doerr HW, Wiese M, Kreuter J, Al-Abed Y, et al. (2010). Anticancer effects of the nitric oxide–modified saquinavir derivative saquinavir-NO against multidrug-resistant cancer cells. *Neoplasia* **12**, 1023–1030.

[26] Hayashi Y, Ueki K, Waha A, Wiestler OD, Louis DN, and von Deimling A (1997). Association of EGFR gene amplification and CDKN2 (p16/MTS1) gene deletion in glioblastoma multiforme. *Brain Pathol* **7**, 871–875.

[27] Michaelis M, Rothweiler F, Klassert D, von Deimling A, Weber K, Fehse B, Kammerer B, Doerr HW, and Cinatl J Jr (2009). Reversal of P-glycoprotein–mediated multidrug resistance by the murine double minute 2 antagonist nutlin-3. *Cancer Res* **69**, 416–421.

[28] Aller S, Yu J, Ward A, Weng Y, Chittaboina S, Zhuo R, Harrell PM, Trinh YT, Qinghai Z, Urbatsch IL, et al. (2009). Structure of P-glycoprotein reveals a molecular basis for poly-specific drug binding. *Science* **323**, 1718–1722.

[29] Bikadi Z, Hazai I, Malik D, Jemnitz K, Veres Z, Hari P, Ni Z, Loo TW, Clarke DM, Hazai E, et al. (2011). Predicting P-glycoprotein-mediated drug transport based on support vector machine and three-dimensional crystal structure of P-glycoprotein. *PLoS One* **6**, e25815.

[30] Waterhouse NJ and Trapani JA (2003). A new quantitative assay for cytochrome *c* release in apoptotic cells. *Cell Death Differ* **10**, 853–855.

[31] Ozvegy-Laczka C, Cserepes J, Elkind NB, and Sarkadi B (2005). Tyrosine kinase inhibitor resistance in cancer: role of ABC multidrug transporters. *Drug Resist Updat* **8**, 15–26.

[32] Shi Z, Peng XX, Kim IW, Shukla S, Si QS, Robey RW, Bates SE, Shen T, Ashby CR Jr, Fu LW, et al. (2007). Erlotinib (Tarceva, OSI-774) antagonizes ATP-binding cassette subfamily B member 1 and ATP-binding cassette subfamily G member 2–mediated drug resistance. *Cancer Res* **67**, 11012–11020.

[33] Kamath AV, Chong S, Chang M, and Marathe PH (2005). P-glycoprotein plays a role in the oral absorption of BMS-387032, a potent cyclin-dependent kinase 2 inhibitor, in rats. *Cancer Chemother Pharmacol* **55**, 110–116.

[34] Michaelis M, Rothweiler F, Agha B, Barth S, Voges Y, Löschmann N, von Deimling A, Breitling R, Doerr HW, Rödel F, et al. (2012). Human neuroblastoma cells with acquired resistance to the p53 activator RITA retain functional p53 and sensitivity to other p53 activating agents. *Cell Death Dis* **3**, e294.

[35] Yankulov KY and Bentley DL (1997). Regulation of CDK7 substrate specificity by MAT1 and TFIIH. *EMBO J* **16**, 1638–1646.

[36] Peterlin BM and Price DH (2006). Controlling the elongation phase of transcription with P-TEFb. *Mol Cell* **23**, 297–305.

[37] Sharma SV, Haber DA, and Settleman J (2010). Cell line-based platforms to evaluate the therapeutic efficacy of candidate anticancer agents. *Nat Rev Cancer* **10**, 241–253.

[38] Haber M, Bordow SB, Haber PS, Marshall GM, Stewart BW, and Norris MD (1997). The prognostic value of MDR1 gene expression in primary untreated neuroblastoma. *Eur J Cancer* **33**, 2031–2036.

[39] de Cremoux P, Jourdan-Da-Silva N, Couturier J, Tran-Perennou C, Schleiermacher G, Fehlbaum P, Doz F, Mosseri V, Delattre O, Klijanienko J, et al. (2007). Role of chemotherapy resistance genes in outcome of neuroblastoma. *Pediatr Blood Cancer* **48**, 311–317.

[40] Pituch-Noworolska A, Zaremba M, and Wieczorek A (2009). Expression of proteins associated with therapy resistance in rhabdomyosarcoma and neuroblastoma tumour cells. *Pol J Pathol* **60**, 168–173.

[41] Dhooge CR, De Moerloose BM, Benoit YC, Van Roy N, Philippé J, and Laureys GG (1997). Expression of the MDR1 gene product P-glycoprotein in childhood neuroblastoma. *Cancer* **80**, 1250–1257.

[42] Carr-Wilkinson J, O'Toole K, Wood KM, Challen CC, Baker AG, Board JR, Evans L, Cole M, Cheung NK, Boos J, et al. (2010). High frequency of p53/MDM2/p14ARF pathway abnormalities in relapsed neuroblastoma. *Clin Cancer Res* **16**, 1108–1118.

[43] Tweddle DA, Pearson AD, Haber M, Norris MD, Xue C, Flemming C, and Lunec J (2003). The p53 pathway and its inactivation in neuroblastoma. *Cancer Lett* **197**, 93–98.

[44] Tweddle DA, Malcolm AJ, Bown N, Pearson AD, and Lunec J (2001). Evidence for the development of p53 mutations after cytotoxic therapy in a neuroblastoma cell line. *Cancer Res* **61**, 8–13.

[45] Keshelava N, Zuo JJ, Waidyaratne NS, Triche TJ, and Reynolds CP (2000). p53 mutations and loss of p53 function confer multidrug resistance in neuroblastoma. *Med Pediatr Oncol* **35**, 563–568.

[46] Keshelava N, Zuo JJ, Chen P, Waidyaratne SN, Luna MC, Gomer CJ, Triche TJ, and Reynolds CP (2001). Loss of p53 function confers high-level multidrug resistance in neuroblastoma cell lines. *Cancer Res* **61**, 6185–6193.

[47] Goldschneider D, Horvilleur E, Plassa LF, Guillaud-Bataille M, Million K, Wittmer-Dupret E, Danglot G, de Thé H, Bénard J, May E, et al. (2006). Expression of C-terminal deleted p53 isoforms in neuroblastoma. *Nucleic Acids Res* **34**, 5603–5612.

[48] Xue C, Haber M, Flemming C, Marshall GM, Lock RB, MacKenzie KL, Gurova KV, Norris MD, and Gudkov AV (2007). p53 determines multidrug sensitivity of childhood neuroblastoma. *Cancer Res* **67**, 10351–10360.

[49] Krystof V, Baumli S, and Fürst R (2012). Perspective of cyclin-dependent kinase 9 (CDK9) as a drug target. *Curr Pharm Des* **18**, 2883–2890.

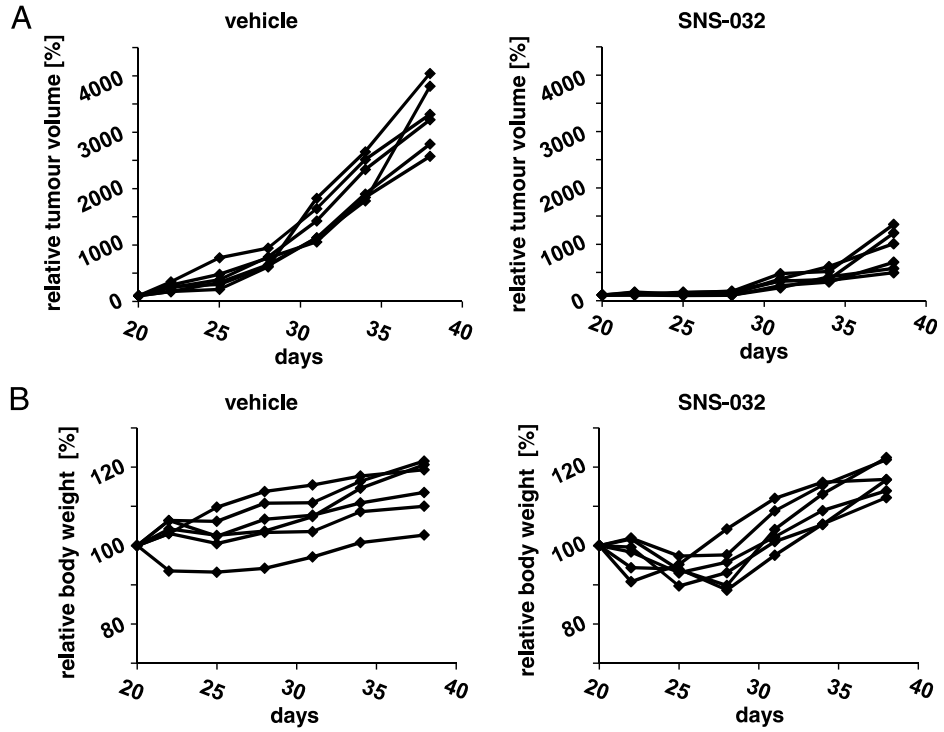

Figure W1. Antineuroblastoma effects of SNS-032 *in vivo*. Effects of SNS-032 (30 mg/kg administered on days 21, 24, and 27) on the growth of subcutaneous UKF-NB-3^{r}CDDP^{1000} (UKF-NB-3 cells with acquired resistance to cisplatin) xenografts (A) and on mice body weights (B) in comparison to vehicle controls.

P-gp Structure	Docking energy of the top four scoring poses (left to right)				Binding site used
3G60	-11.19	-11.05	-10.53	-10.53	Lower QZ59-SSS binding site
3G60	**-12.77**	-12.77	-12.73	-12.62	Lower QZ59-SSS (100 poses) binding site
3G60	-9.03	-8.45	-8.40	-7.93	QZ59-SSS and QZ59-RRR residues
3G60	-12.19	-11.71	-11.50	-11.46	QZ59-RRR binding site
3G60	-8.15	-7.91	-7.71	-7.63	Verapamil binding site
3G61	-10.42	-9.65	-9.50	-9.28	Lower QZ59-SSS binding site
3G61	-10.19	-9.48	-9.21	-9.13	Upper & lower QZ59-SSS residues (100 poses)
3G61	**-12.13**	-11.39	-11.11	-11.04	Upper QZ59-SSS binding site (100 poses)
3G61	-8.51	-8.38	-7.52	-6.58	Upper and lower QZ59-SSS residues
3G61	-11.34	-11.12	-10.88	-10.75	Upper & lower QZ59-SSS residues (100 poses)
3G61	-8.48	-8.31	-8.25	-8.23	Verapamil binding site
3G61	-11.38	-11.04	-10.82	-10.38	Upper QZ59-SSS binding site
3G5U	-9.32	-8.73	-8.30	-8.01	Verapamil binding site
3G5U	-9.02	-8.76	-8.52	-8.02	Lower QZ59-SSS binding site
3G5U	-10.31	-10.22	-9.77	-9.37	Upper QZ59-SSS binding site
3G5U	**-10.79**	-10.39	-9.96	-9.84	Upper & lower QZ59-SSS residues
3G5U	-10.39	-10.13	-9.96	-9.83	Upper & lower QZ59-SSS residues (50 poses)
3G5U	-9.36	-9.12	-8.64	-8.27	Upper QZ59-SSS residues
3G5U	-9.64	-9.15	-8.95	-8.88	Lower QZ59-SSS residues
3G5U	-9.84	-8.90	-8.52	-7.77	QZ59-RRR residues
Human	-9.30	-9.12	-8.94	-8.62	Verapamil binding site
Human	**-10.63**	- 10.49	- 9.44	- 9.36	Lower QZ59-SSS residues
Human	- 9.99	- 9.55	- 9.01	- 9.00	Upper & lower QZ59-SSS residues
Human	- 10.40	- 10.08	- 10.00	- 9.55	Upper & lower QZ59-SSS residues (100 poses)
Human	**- 10.62**	- 10.47	- 10.17	- 9.99	Upper QZ59-SSS residues (100 poses)
Human	**-10.70**	- 10.58	- 9.93	- 9.28	Upper QZ59-SSS binding site
Human	**-10.66**	-10.24	-9.35	-9.30	Upper QZ59-SSS residues
Human	-10.44	-10.26	-9.76	-9.39	Upper QZ59-SSS residues (100 poses)
Human	-9.20	-9.04	-8.98	-8.64	Lower QZ59-SSS residues
Human	-10.54	-9.23	-9.15	-8.74	QZ59-RRR residues
3G60	**-10.67***	**-10.38***	**-10.17***	**-10.03***	Average of all binding sites
3G61	-10.35	-9.91	-9.61	-9.34	Average of all binding sites
3G5U	-9.83[L]	-9.43[L]	-9.08[L]	-8.75[L]	Average of all binding sites
Human	-10.25	-9.91	-9.47	-9.19	Average of all binding sites

*: The best average score; [L]: the worst average score

Figure W2A. Docking studies on the interaction of SNS-032 with ABCB1. SNS-032 was docked into the homology model of human ABCB1 and the three X-ray structures of mouse Abcb1a, with the binding sites defined using the positions of the co-crystallized ligands, QZ59-RRR and QZ59-SSS (amino acid residues within 4.5-Å distance), and the verapamil binding site (residues protected from MTS labeling by verapamil) as described by Aller et al. [28]. (A) A summary of the top-scoring poses. Using all binding site definitions, docking into 3G60 and 3G61, which are the structures of ABCB1 with co-crystallized ligands, generated consistently better binding scores than docking 3G5U, the structure crystallized in the absence of a ligand. The best binding scores in all cases were achieved when the biding site was defined using the co-crystallized QZ59-SSS. Results indicated that the basic scaffold of SNS-032 makes several strong bonds at the binding pocket of QZ59-SSS. The top 30 retained poses for each binding pocket showed consistency in terms of the amino acids involved in the interaction (B). (C) A list of the interactions for the top poses. These interacting residues sit in transmembrane helices 7, 10, 11, and 12. They are all within the list of residues facing the internal cavity of ABCB1 within the lipid bilayer as described by Aller et al. [28]. The only exception from this is Ser-725, which, in 3 of 30 poses, is involved in hydrogen bonding with the nitrogen atom of the thiazole ring in 3G60 structure (B and D). SNS-032 was docked into different binding sites of ABCB1 structures (mouse and human). The flexibility and polyspecificity of ABCB1 can lead to the uncertainty of scoring functions. Therefore, docking studies in this work considered sampling a large number of docking poses incorporating four different protein structures with four different binding site definitions in each structure. The results identified residues in the binding sites that were involved in a high number of docking poses (>10%). These amino acids are all part of the internal cavity of ABCB1 within the lipid bilayer with only one exception and sit within transmembrane helices 1, 3, 5, 6, 7, 11, and 12 (E). The preferential binding site for SNS-032 was suggested to be close to the binding site of cyclic-tris-(*S*)-valineselenazole (QZ59-SSS) in the mouse Abcb1a X-ray structures and the human homology model of this protein. Our results indicate several strong hydrogen bonding interactions in mouse and human ABCB1 (D and F), which is a characteristic of the more hydrophilic lower QZ59-SSS binding site. These are accompanied by several H-Pi and Pi-Pi interactions including interactions between Val-982 of human ABCB1 (also protected from MTS labeling by verapamil) and oxazole ring and Phe-978 and dimethylpropane group (D). Protein interaction energies (kcal/mol) of the four top-scoring poses; binding site is that of verapamil, the cyclic hexapeptide inhibitors (QZ59-RRR and QZ59-SSS) separately, or the residues involved in both QZ59-RRR and QZ59-SSS binding sites. Number of poses retained was 30 or higher. The highest interaction energies are highlighted in bold.

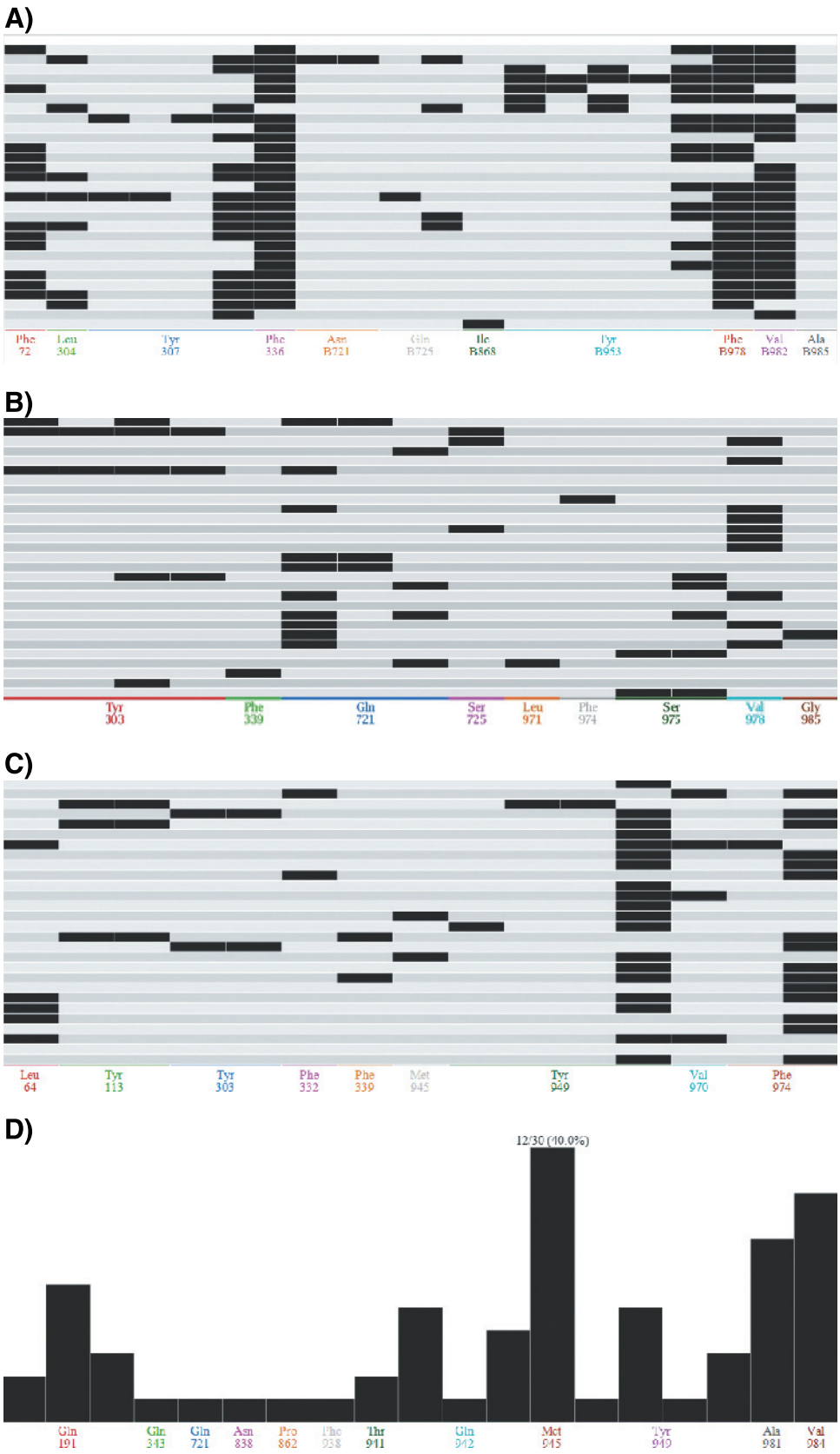

Figure W2B. The population histogram for the 30 SNS-032/ABCB1 docking poses at the QZ59-SSS binding site. Complexes are shown along the *Y*-axis, and the residues corresponding to each group of fingerprint bits on the *X*-axis are coded with an arbitrary sequence of colors. (A) Human model of ABCB1. (B) 3G60. (C) 3G61. (D) 3G5U.

Fragment of the Ligand	Receptor	Interaction	Distance (Å)	E (kcal/mol)
Mouse P-gp model (3G60)				
Nitrogen in Thiazole	Ser725	H-acceptor	3.47	-0.7
Piperidine	Gln721	H-acceptor	3.10	-1.9
Thiazole	Val978	pi-H	3.44	-0.9
Thiazole	Phe728	pi-pi	3.92	-0.0
Oxazole	Phe 974	pi-pi	3.68	-0.0
Mouse P-gp model (3G61)				
Oxazole	Phe953	H-pi	3.53	-0.6
Carbon in piperidine	Phe974	pi-pi	3.56	-0.0
Mouse P-gp model (3G5U)				
Thiazole	Ala865	pi-H	3.15	-1.4
Human P-gp model (by Bikadi)				
Piperidine	Asn721 (717 in mouse)	H-donor	2.98	-0.9
Dimethylpropane	Phe978 (974 in mouse)	H-pi	3.48	-0.6
Oxazole	Val982 (978 in mouse)	pi-H	3.34	-0.7

Figure W2C. Ligand interactions report for SNS-032 at the first pose using QZ59-SSS lower binding site.

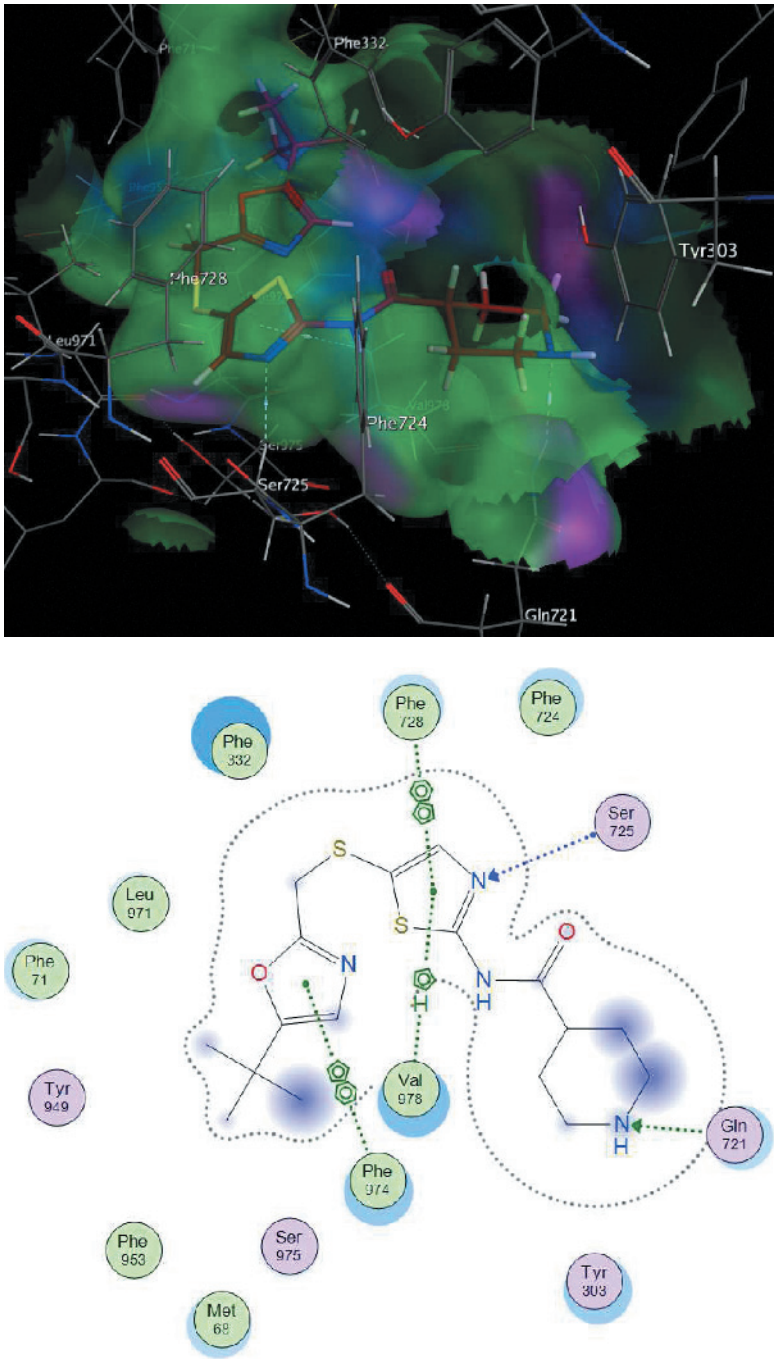

Figure W2D. Interaction of SNS-032 with QZ59-SSS binding site of 3G60 using MOE software. Ligand interaction 2D diagrams indicate the polar and nonpolar interactions by pink or green amino acids, hydrogen bonding by green dotted arrows, and Pi-H interactions with green dotted line. In this diagram, the energy cutoff for H-bond and ionic interactions was −0.5 kcal/mol and the maximum distance for nonbonded groups was 4.5 Å. Proximity contours are dotted lines surrounding the ligand and indicate the shape of the binding site and available space to the more outward-facing parts of the ligand. Blue shadows in some amino acids indicate the receptor exposure differences by the size and intensity of the quoits disks. The directions of the shadow indicate the directions of the amino acids toward the ligands. The blue clouds around the ligand atoms indicate the solvent exposure.

Human		3G60		3G61		3G5U	
Residue	TM	Residue	TM	Residue	TM	Residue	TM
Phe72 (Phe71)	1	Tyr303	5	Leu64	1	Gln191	3
Phe336 (Phe332)	6	Gln721	7	Tyr949	11	Thr941	11
Tyr953 (Tyr949)	11	Ser975	12	Phe974	12	Gln942	11
Phe978 (Phe974)	12	Val978	12			Met945	11
Val982 (Val978)	12					Tyr949	11
						Ala981	12
						Val984*	12

*: Not in the list of the residues within the internal cavity of ABCB1 within the lipid bilayer as described by Aller et al (2009)

Figure W2E. The most common interacting residues with SNS-032 in docking poses and their location in the transmembrane helices of ABCB1; residues in brackets are residue numbers in mouse.

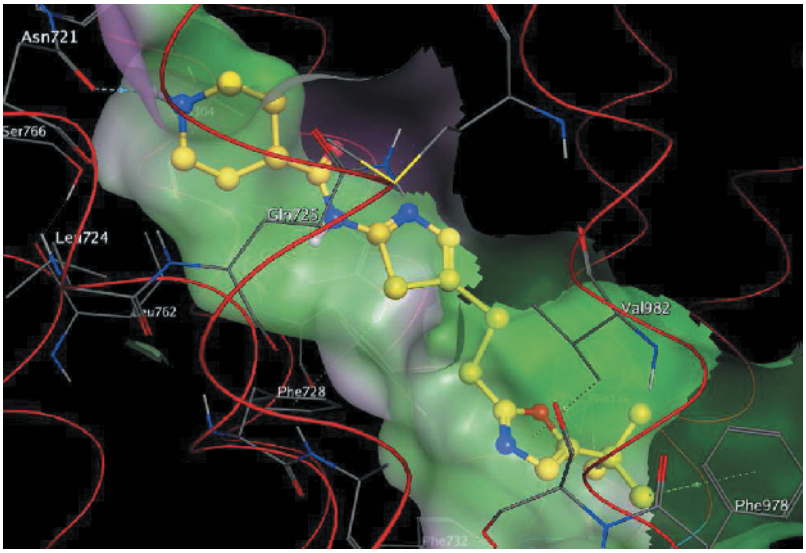

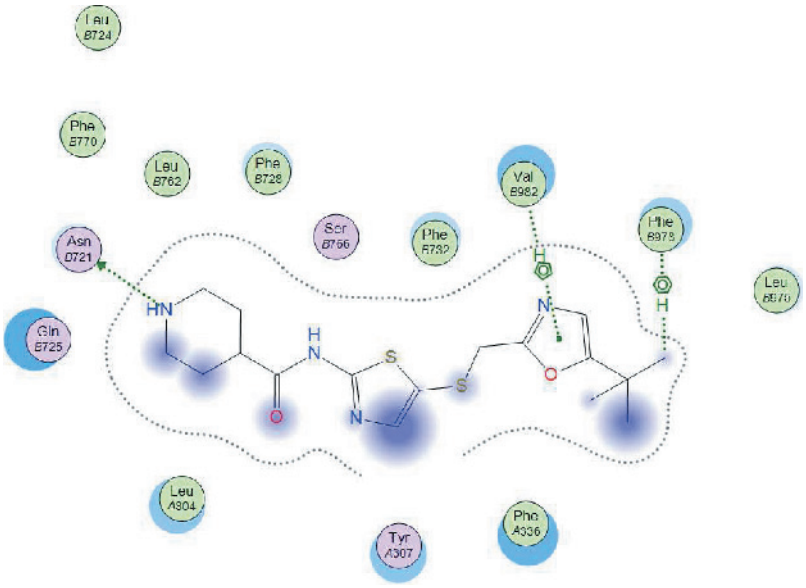

Figure W2F. Interaction of SNS-032 with verapamil binding site of human ABCB1 using MOE software. Ligand interaction 2D diagrams indicate the polar and nonpolar interactions by pink or green amino acids, hydrogen bonding by green dotted arrows, and Pi-H interactions with green dotted line. In this diagram, the energy cutoff for H-bond and ionic interactions was −0.5 kcal/mol and the maximum distance for nonbonded groups was 4.5 Å. Proximity contours are dotted lines surrounding the ligand and indicate the shape of the binding site and available space to the more outward-facing parts of the ligand. Blue shadows in some amino acids indicate the receptor exposure differences by the size and intensity of the quoits disks. The directions of the shadow indicate the directions of the amino acids toward the ligands. The blue clouds around the ligand atoms indicate the solvent exposure [28].

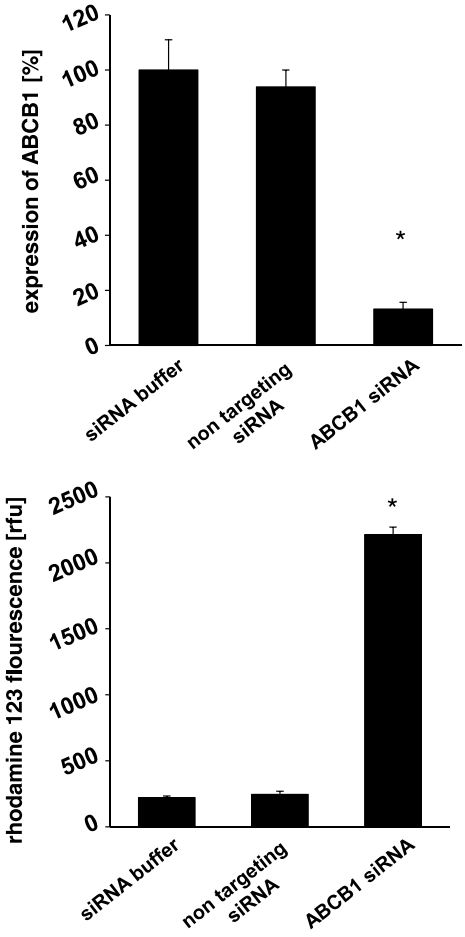

Figure W3. siRNA-mediated depletion of ABCB1 in UKF-NB-3^{ABCB1} cells. ABCB1 expression and accumulation of the fluorescent ABCB1 substrate rhodamine 123 in UKF-NB-3ABCB1 cells 48 hours after transfection with siRNA directed against ABCB1. *$P < .05$ relative to control.

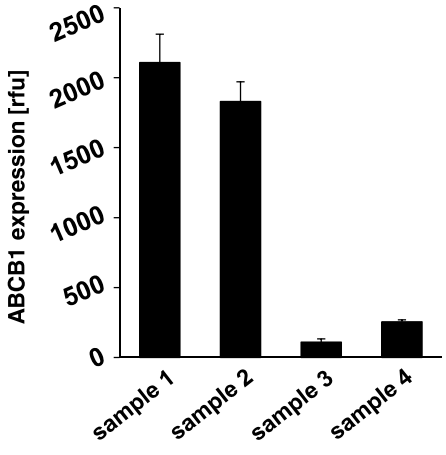

Figure W4. ABCB1 expression in primary neuroblastoma samples.

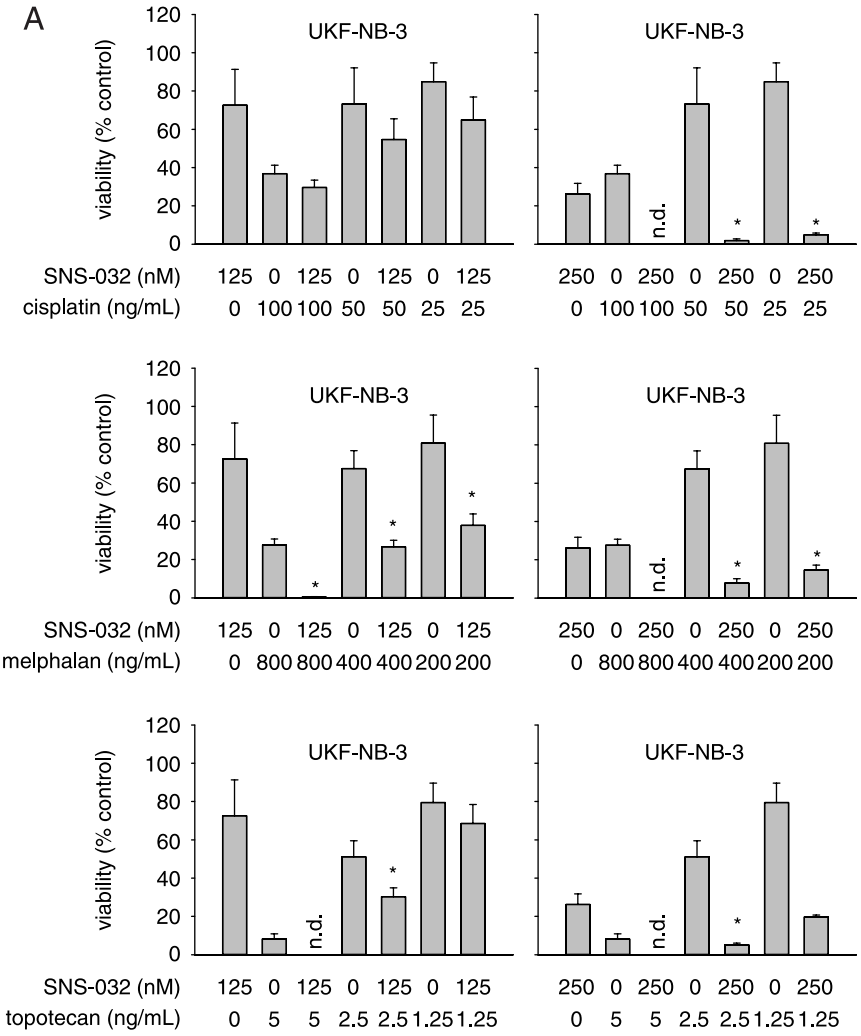

Figure W5. (A) Antineuroblastoma activity of SNS-032 in combination with cytotoxic anticancer drugs in UKF-NB-3 cells. Cell viability was determined relative to nontreated control cells by MTT after 5 days of incubation. *$P < .05$ relative to SNS-032 and cytotoxic drug; n.d., not detectable cell viability. (B) Antineuroblastoma activity of SNS-032 in combination with cytotoxic anticancer drugs in UKF-NB-3 cells resistant to cisplatin (UKF-NB-3^{r}CDDP^{1000}), melphalan (UKF-NB-3^{r}MEL^{400}), or topotecan (UKF-NB-3^{r}TOPO^{15}). Cell viability was determined relative to nontreated control cells by MTT after 5 days of incubation. *$P < .05$ relative to SNS-032 and cytotoxic drug; n.d., not detectable cell viability.

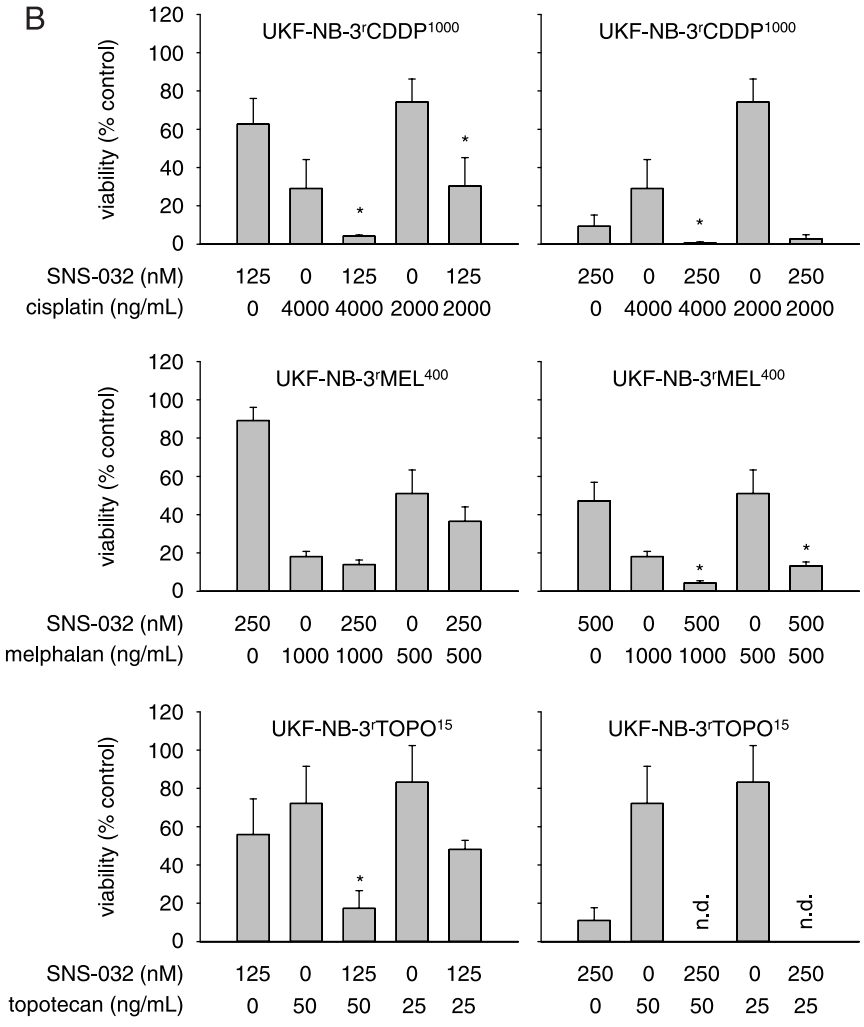

Figure W5. (*continued*).